Video Article

Crystal Structure of the N-terminal Domain of Ryanodine Receptor from *Plutella xylostella*

Bidhan Chandra Nayak[1], Jie Wang[1], Lianyun Lin[1,2,3,4], Weiyi He[2,3,4], Minsheng You[2,3,4], Zhiguang Yuchi[1,2]

[1]Tianjin Key Laboratory for Modern Drug Delivery & High-Efficiency, Collaborative Innovation Center of Chemical Science and Engineering, School of Pharmaceutical Science and Technology, Tianjin University

[2]State Key Laboratory of Ecological Pest Control for Fujian/Taiwan Crops and Institute of Applied Ecology, Fujian Agriculture and Forestry University

[3]Joint International Research Laboratory of Ecological Pest Control, Ministry of Education, Fuzhou

[4]Fujian-Taiwan Joint Centre for Ecological Control of Crop Pests, Fujian Agriculture and Forestry University

Correspondence to: Minsheng You at msyou@iae.fjau.edu.cn, Zhiguang Yuchi at yuchi@tju.edu.cn

URL: https://www.jove.com/video/58568
DOI: doi:10.3791/58568

Keywords: Biochemistry, Issue 141, protein expression, purification, crystallization, x-ray crystallography, molecular replacement, ryanodine receptor, diamondback moth

Date Published: 11/30/2018

Citation: Nayak, B.C., Wang, J., Lin, L., He, W., You, M., Yuchi, Z. Crystal Structure of the N-terminal Domain of Ryanodine Receptor from *Plutella xylostella*. *J. Vis. Exp.* (141), e58568, doi:10.3791/58568 (2018).

Abstract

Development of potent and efficient insecticides targeting insect ryanodine receptors (RyRs) has been of great interest in the area of agricultural pest control. To date, several diamide insecticides targeting pest RyRs have been commercialized, which generate annual revenue of 2 billion U.S. dollars. But comprehension of the mode of action of RyR-targeting insecticides is limited by the lack of structural information regarding insect RyR. This in turn restricts understanding of the development of insecticide resistance in pests. The diamondback moth (DBM) is a devastating pest destroying cruciferous crops worldwide, which has also been reported to show resistance to diamide insecticides. Therefore, it is of great practical importance to develop novel insecticides targeting the DBM RyR, especially targeting a region different from the traditional diamide binding site. Here, we present a protocol to structurally characterize the N-terminal domain of RyR from DBM. The x-ray crystal structure was solved by molecular replacement at a resolution of 2.84 Å, which shows a beta-trefoil folding motif and a flanking alpha helix. This protocol can be adapted for the expression, purification and structural characterization of other domains or proteins in general.

Video Link

The video component of this article can be found at https://www.jove.com/video/58568/

Introduction

Ryanodine receptors (RyRs) are specific ion channels, which mediate the permeation of Ca^{2+} ions across the sarcoplasmic reticulum (SR) membranes in muscle cells. Therefore, they play an important role in the excitation contraction coupling process. In its functional form, RyR assembles as a homo-tetramer with a molecular mass of >2 MDa, with each subunit comprising of ~5000 amino acid residues. In mammals, there are three isoforms: RyR1- skeletal muscle type, RyR2- cardiac muscle type and RyR3- ubiquitously expressed in different tissues[1].

In insects there is only one type of RyR, which is expressed in muscular and nervous tissue[2]. Insect RyR is more similar to mammalian RyR2 with a sequence identity of about 47%[3]. Diamide insecticides targeting RyR of Lepidoptera and Coleoptera have been developed and marketed by major companies like Bayer (flubendiamide), DuPont (chlorantraniliprole) and Syngenta (cyantraniliprole). Since its relatively recent launch, diamide insecticides have become one of the fastest growing class of insecticides. Currently, the sales of these three insecticides annually have crossed 2 billion U.S. dollars with a growth rate of more than 50% since 2009 (Agranova).

Recent studies have reported the development of resistance in insects after a few generations of usage of these insecticides[4,5,6,7,8]. The resistance mutations in the transmembrane domain of RyRs from the diamondback moth (DBM), *Plutella xylostella* (G4946E, I4790M) and the corresponding positions in tomato leafminer, *Tuta absoluta* (G4903E, I4746M) show that the region might be involved in diamide insecticide binding as this region is known to be critical for gating of the channel[4,8,9]. Despite extensive research in this area, the exact molecular mechanisms of diamide insecticides remain elusive. Moreover, it is unclear whether the resistance mutations affect the interactions with diamides directly or allosterically.

Earlier studies have reported the structure of several RyR domains from mammalian species and the structure of full-length mammalian RyR1 and RyR2 by x-ray crystallography and cryo-electron microscopy, respectively[10,11,12,13,14,15,16,17,18,19,20,21]. But so far, no structure of insect RyR has been reported, which prohibits us from understanding the molecular intricacies of the receptor function as well as the molecular mechanisms of insecticide action and development of insecticide resistance.

In this manuscript, we present a generalized protocol for the structural characterization of N-terminal β-trefoil domain of ryanodine receptor from the diamondback moth, a destructive pest infecting cruciferous crops worldwide[22]. The construct was designed according to the published rabbit

RyR1 NTD crystal structures[23,24] and the cryo-EM structural models[16,17,18,19,20,21]. This is the first high-resolution structure reported for insect RyR, which reveals the mechanism for channel gating and provides an important template for the development of species-specific insecticides using structure-based drug design. For structure elucidation, we employed x-ray crystallography, which is considered as the 'gold standard' for protein structure determination at near atomic resolution. Although the crystallization process is unpredictable and labor intensive, this step-by-step protocol will help researchers to express, purify and characterize other domains of insect RyR or any other proteins in general.

Protocol

1. Gene Cloning, Protein Expression, and Purification

1. PCR amplify DNA corresponding to protein of interest (residues 1-205 of DBM RyR, Genbank acc. no. AFW97408) and clone into pET-28a-HMT vector by Ligation-Independent Cloning (LIC)[25]. This vector contains a histidine tag, MBP tag and a TEV protease cleavage site at the N-terminus[15].
    1. Design LIC primers for amplification of target gene with LIC-compatible 5' extensions:
    Forward LIC primer:
    5' TACTTCCAATCCAATGCAATGGCGGAAGCGGAAGGGG 3'
    Reverse LIC primer:
    5' TTATCCACTTCCAATGTTATTATATGCCGGTCCCGTACGGC 3'
    2. Combine the reaction components (50 µL): 1 µL of DNA templates (100 ng/µL), 1 µL of forward primer (10 µM), 1 µL of reverse primer (10 µM), 0.5 µL of DNA polymerase (NEB), 5 µL of 10x reaction buffer, 1 µL of dNTP (25 mM), 40.5 µL of RNase free ddH_2O.
        1. Place the reaction mixture in a PCR machine and run the following program.
        2. Incubate at 95 °C for 3 min, and then run 30 cycles of (95 °C for 30 s, 58 °C for 15 s, 72 °C for 1 min). Incubate at 72 °C for 5 min and then hold at 4 °C.
        3. Run the entire reaction mix (50 µL) on a 2% agarose gel and extract with a Gel Extraction Kit. Follow manufacturer's protocol.
    3. Ligation-Independent Cloning (LIC)
        1. Perform SspI digestion (60 µL): 20 µL of vector DNA (50 ng/µL), 6 µL of 10x reaction buffer, 4 µL of SspI, and 30 µL of ddH_2O. Incubate at 37 °C for 3 h. Run the entire reaction mix on 1% agarose gel and extract with a Gel Extraction Kit. Follow manufacturer's protocol.
        2. Perform T4 DNA Polymerase treatment of the vector and insert DNA. Combine the following: 5 µL of vector or insert DNA (50 ng/µL), 2 µL of 10x T4 DNA Polymerase Buffer, 1 µL of dGTP (25 mM) for vector or 1 µL of dCTP (25 mM) for insert DNA, 1 µL of DTT (100 mM), 0.4 µL of T4 DNA Polymerase (LIC-qualified), and 9.6 µL of ddH_2O. Incubate reactions at room temperature for 40 min. Heat-inactivate enzyme at 75 °C for 20 min.
        Note: The LIC vector and insert DNA must be treated in separate reactions.
        3. Perform the LIC annealing reaction. Combine the following: 2 µL of T4-treated insert DNA, 2 µL of T4-treated LIC vector DNA. Incubate reaction at room temperature for 10 min.

2. Transform BL21 (DE3) *E. coli* cells with this recombinant plasmid.
    1. Thaw competent cells (50 µL in micro-centrifuge tube) on ice.
    2. Add approximately 1 µL (50 ng) of plasmid into the tube. Mix the cells and DNA by gently flicking the tube 2–3 times. Place the tube on ice for 20 min.
    3. Heat shock at 42 °C for 40 s. Place the tube on ice again for 2 min. Add 1 mL of room temperature LB media to the tube.
    4. Place the mixture tube in the 250 rpm shaker at 37 °C for 45 min. Spread 150–200 µL of the mixture onto the selection plates. Invert the plate and incubate overnight at 37 °C.

3. Pick a single colony and culture the cells in 100 mL 2YT medium containing 50 µg/mL kanamycin at 37 °C overnight. Next morning, inoculate 1 L 2YT medium containing 50 µg/mL kanamycin with 10 mL of overnight culture and incubate in 37 °C shaker incubator at 250 rpm, until the OD_{600} reaches ~0.6. Thereafter induce the culture with IPTG to a final concentration of 0.4 mM and grow for another 5 h at 30 °C.
4. Harvest the cells by centrifugation at 8,000 x *g* for 10 min at 4 °C, collect the cells and resuspend every 10 g cells in 40 mL lysis buffer (10 mM HEPES pH 7.4, 250 mM KCl, 10 mM β-mercaptoethanol, 25 µg/mL lysozyme, 25 µg/mL DNase, 1 mM PMSF).
    1. Disrupt it by sonication at 65% amplitude for 8 min with 1 s on and 1 s off. Remove the cell debris by centrifugation at 40,000 x *g* for 30 min at 4 °C. Filter the supernatant by passing through 0.22 µm filter and load it into the sample loop.

5. Purify the fusion protein, cleave the tag and re-purify the target protein.
    1. Purify the fusion protein using Ni-NTA column (binding buffer: 10 mM HEPES pH 7.4, 250 mM KCl; elution buffer: 10 mM HEPES pH 7.4, 250 mM KCl, 500 mM imidazole) and purify by a purification system, with a linear gradient of 20–250 mM imidazole.
    2. Cleave the eluted target protein with TEV protease (1:50 ratio) overnight at 4 °C.
    3. Purify the cleavage reaction mixture by using amylose resin column (binding buffer: 10 mM HEPES pH 7.4, 250 mM KCl; elution buffer: 10 mM HEPES pH 7.4, 250 mM KCl, 10 mM maltose) and Ni-NTA column to remove the tag and TEV protease. The target protein will be in the flow-through fraction of these two columns.
    4. Dialyze the sample against dialysis buffer (10 mM Tris-HCl pH 8.8, 50 mM KCl, 10 mM β-mercaptoethanol to reduce the salt concentration. Purify the sample on a anion exchange column (binding buffer: 10 mM Tris-HCl pH 8.8, 10 mM β-mercaptoethanol; elution buffer: 10 mM Tris-HCl pH 8.8, 1 M KCl, 10 mM β-mercaptoethanol) by a linear gradient of 20–500 mM KCl in the elution buffer.
    5. As a final step in the purification process, concentrate the protein using centrifugal concentrator (10 kDa MWCO) and inject into a Superdex 200 26/600 gel-filtration column to check the homogeneity.

6. Examine the purity of the protein by running it on a 15% SDS PAGE.

NOTE: All columns are running on a protein purification system with a binding flow rate of 2 mL/min, and an elution flow rate of 4 mL/min except for gel-filtration at 1 mL/min.

2. Protein Preparation and Crystallization

1. Concentrate the purified protein sample to 10 mg/mL using centrifugal concentrator (10 kDa MWCO) and buffer exchange to crystallization buffer before storing at -80 °C.
2. Perform crystallization screening (1:1 ratio, 200 nL of protein and 200 nL of reservoir buffer) by the sitting drop vapor diffusion method at 295 K with several crystallization kits using an automated liquid handling robotic system in a 96-well format.
   NOTE: We used kits from Molecular Dimensions and Hampton research and the Gryphon automated liquid handling system.
3. Seal the 96-well crystallization plate to prevent evaporation and enable the equilibration of the protein drop with the reservoir buffer. Then keep the plates in the crystal incubator at 18 °C.
4. Check the 96-well plates periodically using a light microscope to monitor crystal formation and growth.
5. To differentiate protein crystals from salt crystals, use a protein dye. Add 1 µL of dye to the target drop. Wait for about 1 h and observe under microscope. The protein crystals will turn blue.
6. Use the positive crystallization conditions (1.5 M ammonium sulfate, 0.1 M Tris pH 8.0) to further optimize the crystals using hanging drop vapor-diffusion method in 24-well plates.
   1. Optimize pH from 7.0 to 8.5 with 0.5 pH unit interval every step. Optimize concentration of ammonium sulfate from 1.2 M to 1.7 M with 0.1 M interval every step. (In our case the best condition producing large plate-shaped crystals was 0.1 M HEPES pH 7.0 and 1.6 M ammonium sulfate)

3. Crystal Mounting, X-Ray Data Collection, and Structure Determination

1. Mount crystals in a cryoloop and flash-cool in liquid nitrogen using reservoir solution containing 20% glycerol as cryo-protectant. Place the crystals in unipuck for storage and transportation.
2. Pre-screen protein crystals using a Rigaku in-house X-ray diffractor. Choose the best ones with the highest resolutions for data collection at synchrotron facilities (our dataset was collected from BL17U1 at Shanghai Synchrotron Radiation Facility).
   1. Use the beamline control software BluIce[26] to mount and center the crystals by automatic or manual centering function. Perform test exposures to determine the data collection strategy, including starting angle, exposure time, detector distance, frame width and numbers.
   2. Collect dataset accordingly (we collected 180 frames with 1 s exposure time, 1° frame width and the detector distance of 350 mm).
3. Index, integrate and scale the dataset using HKL2000 suite[27]. First carry out the peak search function to find the diffraction spots, and then index the spots and select the right space group. After peak integration, scale the dataset with the proper error model and save the output .sca file.
4. Solve the phase problem by molecular replacement using Phaser[28] in PHENIX[29].
   1. Calculate the possible copy number of protein molecules in the asymmetric unit by Xtriage[30].
   2. Look for the proper structure templates with high sequence identity and structural similarity as the target protein using known structures from literature or the models generated by structure prediction server such as Phyre2[31] (we used rabbit RyR1 NTD as a search model, PDB ID 2XOA).
   3. Run Phaser using the diffraction data file, the template structure file and the protein sequence file to find the solution.
5. Perform AutoBuild[32] in PHENIX[29] to generate the initial model using the output file from Phaser and the sequence file from the target protein.
6. Manually build the structure into the modified experimental electron density using Coot[33] and refine using phenix.refine[34] in iterative cycles.
7. Validate the final model using the validation tools in PHENIX[18].

Representative Results

Purification

The N-terminal domain of DBM RyR was expressed as a fusion protein with a hexahistidine tag, a MBP tag and a TEV protease cleavage site. We followed a five-step purification strategy to obtain a highly pure protein, suitable for crystallization purpose. At first, the fusion protein was purified from the soluble fraction of cell lysate by Ni-NTA column (HisTrap HP). Next, the fusion protein was subjected to TEV protease cleavage and the hexahistidine-MBP moiety was removed by amylose resin column followed by Ni-NTA column. Further, the protein was purified by anion exchange column (Q Sepharose HP) and finally by gel-filtration column (Superdex 200 26/600). The final yield of purified protein from 1 L bacterial culture using 2YT media was ~4 mg. The purified protein showed a single band on SDS-PAGE at ~21 kDa (**Figure 1**). The elution volume from gel-filtration column confirmed the purified RyR NTD to be a monomer (**Figure 1**).

Crystallization

Initial crystallization screening in 96-well plates yielded crystals in several conditions. These conditions were selected for crystal optimization in 24 well plates. The most optimal condition where high quality plate-shape crystals were formed was 0.1 M HEPES pH 7.0 and 1.6 M ammonium sulfate (**Figure 2**).

Structure determination

Crystals obtained was diffracted to 2.84 Å on beamline BL17U1 at Shanghai Synchrotron Radiation Facility. The crystal was indexed in space group $P6_1$ with unit-cell parameters a = 170.13, b = 170.13, c = 51.763 Å, α = β = 90.00°, γ = 120°. For structure determination, molecular replacement was employed using rabbit RyR1 NTD as a search model in PHENIX. Further refinement of the structure was done in PHENIX to a final R_{work} and R_{free} of 21.63 and 24.52%, respectively. The data collection and refinement statistics are listed in **Table 1**. The solved structure of DBM RyR NTD covering the residues 1-205 (PDB ID 5Y9V) is shown in **Figure 3**.

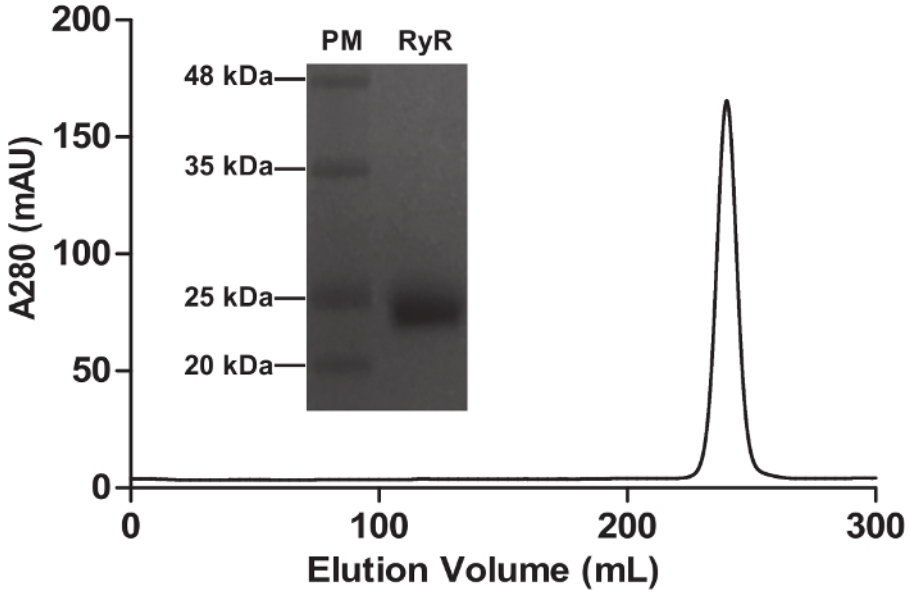

Figure 1: SDS-PAGE and gel filtration chromatogram representing purification of DBM RyR NTD[35]. SDS PAGE (15%) in the inset shows purified DBM RyR NTD as a single band after the five step purification strategy. The left lane shows standard protein marker (PM). The gel filtration chromatogram obtained using a Superdex 200 26/600 column shows the elution peak at 240 mL, which corresponds to the monomeric form of the protein. Please click here to view a larger version of this figure.

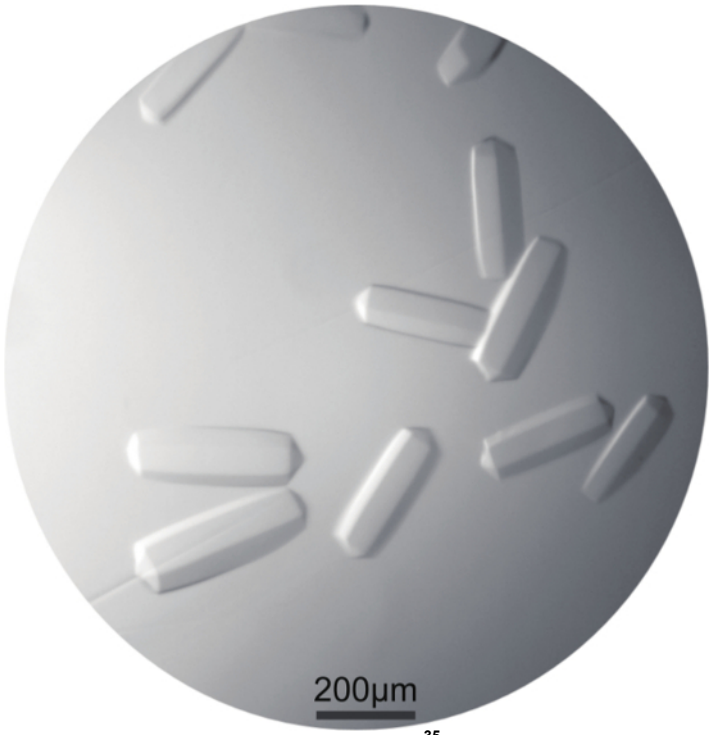

Figure 2. Crystallization of DBM RyR NTD[35]. Crystals of DBM RyR NTD produced by vapor-diffusion method as seen under a light microscope. The crystallization condition was 0.1 M HEPES pH 7.0 and 1.6 M ammonium sulfate. Scale bar = 200 µm. Please click here to view a larger version of this figure.

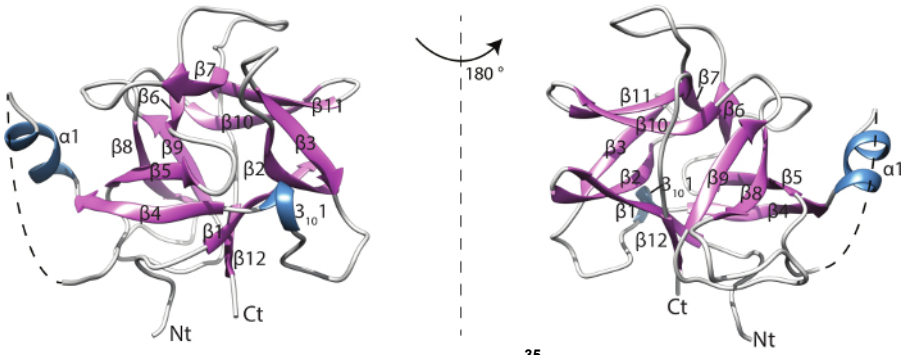

Figure 3: Structure of DBM RyR NTD (PDB ID 5Y9V)[35]. Solved structure of the protein shown from two views. Secondary structure elements are labeled. β strands are shown in purple. α helix and a 3_{10} helix are shown in blue. Loops are shown in white. Nt and Ct represent the N-terminal and C-terminal of the protein, respectively. Please click here to view a larger version of this figure.

Table 1: Data collection and refinement statistics for the DBM RyR NTD crystal[35]. Please click here to download this table.

Discussion

In this paper, we describe the procedure to recombinantly express, purify, crystallize and determine the structure of DBM RyR NTD. For crystallization, a crucial requirement is to obtain proteins with high solubility, purity and homogeneity. In our protocol, we chose to use pET-28a-HMT vector as it contains a hexahistidine tag and MBP tag, both of which could be utilized for purification to obtain a higher fold purity. Additionally, the MBP tag aids in the solubility of the target protein. We purified the protein by five consecutive steps which yielded protein that was highly pure and suitable for crystallization. Crystallization screening was performed using automated liquid handling system. Compared to traditional screening by manual drop setting, automated system uses very small volumes of sample, saves time and energy. It also enhances reproducibility due to accuracy of liquid handling. Crystals were diffracted in-house for screening and at synchrotron for data collection as it provides x-ray with higher intensity and less divergence, thereby yielding high quality data. Molecular replacement was our first choice as similar structural templates were available in the database. The alternative way is to use experimental phasing, including MAD, SAD, MIR, *etc.*

While solving the structure of DBM RyR NTD, the Matthews coefficients obtained from Xtriage[30] suggested that the asymmetric unit (ASU) most likely contained four monomers with 46% solvent content, which has a probability of 49%. However, we could not find the right solution with four molecules in ASU. Subsequent runs to look for two, three, five, six molecules also failed. Eventually we found the right solution with only one molecule in ASU, which only has 4% probability and over 86% solvent content. The high water content was confirmed after we solved the structure. Thus, the extreme high solvent content does exist depending on the intrinsic way in which protein packs.

Although X-ray crystallography is a gold-standard in protein structure determination, proteins with large disorder or flexible regions and some large protein complexes with weak affinity are challenging to crystallize. Protein engineering methods, including loop-truncation, surface entropy reduction and cross-linking, might improve the chance of obtaining better protein crystals. Besides the revealing of high-resolution protein structures, X-ray crystallography can also be used to study the protein-pesticide interactions, which would help us on structure-based pesticide design. Qi *et al.* found that different families of diamides might bind to distinct sites that are different across species[36]. Using our strategy, one can determine the RyR structures from multiple species and identify the unique elements responsible for the observed species-specificity. Overall, this protocol can be adapted for expression, purification, crystallization and structure determination of any proteins or protein domains by themselves or in complex with small molecule drugs.

Disclosures

The authors have nothing to disclose.

Acknowledgements

Funding for this research was provided by: National Key Research and Development Program of China (2017YFD0201400, 2017YFD0201403), National Nature Science Foundation of China (31320103922, 31230061), and Project of National Basic Research (973) Program of China (2015CB856500, 2015CB856504). We are grateful to the staff on the beamline BL17U1 at Shanghai Synchrotron Radiation Facility (SSRF).

References

1. Giannini, G., & Sorrentino, V. Molecular structure and tissue distribution of ryanodine receptors calcium channels. *Medicinal Research Reviews.* **15** (4), 313-323 (1995).
2. Takeshima, H. *et al.* Isolation and characterization of a gene for a ryanodine receptor/calcium release channel in Drosophila melanogaster. *FEBS Letters.* **337** (1), 81-87 (1994).
3. Sattelle, D. B., Cordova, D., & Cheek, T. R. Insect ryanodine receptors: molecular targets for novel pest control chemicals. *Invertebrate Neuroscience.* **8** (3), 107-119 (2008).
4. Steinbach, D. *et al.* Geographic spread, genetics and functional characteristics of ryanodine receptor based target-site resistance to diamide insecticides in diamondback moth, Plutella xylostella. *Insect Biochemistry and Molecular Biology.* **63** 14-22 (2015).

5. Wang, X., Khakame, S. K., Ye, C., Yang, Y., & Wu, Y. Characterisation of field-evolved resistance to chlorantraniliprole in the diamondback moth, Plutella xylostella, from China. *Pest Management Science.* **69** (5), 661-665 (2013).
6. Liu, X., Wang, H. Y., Ning, Y. B., Qiao, K., & Wang, K. Y. Resistance Selection and Characterization of Chlorantraniliprole Resistance in Plutella xylostella (Lepidoptera: Plutellidae). *Journal of Economic Entomology.* **108** (4), 1978-1985 (2015).
7. Guo, L. *et al.* Functional analysis of a point mutation in the ryanodine receptor of Plutella xylostella (L.) associated with resistance to chlorantraniliprole. *Pest Management Science.* **70** (7), 1083-1089 (2014).
8. Troczka, B. *et al.* Resistance to diamide insecticides in diamondback moth, Plutella xylostella (Lepidoptera: Plutellidae) is associated with a mutation in the membrane-spanning domain of the ryanodine receptor. *Insect Biochemistry and Molecular Biology.* **42** (11), 873-880 (2012).
9. Roditakis, E. *et al.* Ryanodine receptor point mutations confer diamide insecticide resistance in tomato leafminer, Tuta absoluta (Lepidoptera: Gelechiidae). *Insect Biochemistry and Molecular Biology.* **80** 11-20 (2017).
10. Borko, L. *et al.* Structural insights into the human RyR2 N-terminal region involved in cardiac arrhythmias. *Acta Crystallographica Section D.* **70** (Pt 11), 2897-2912 (2014).
11. Sharma, P. *et al.* Structural determination of the phosphorylation domain of the ryanodine receptor. *FEBS Journal.* **279** (20), 3952-3964 (2012).
12. Kimlicka, L., Lau, K., Tung, C. C., & Van Petegem, F. Disease mutations in the ryanodine receptor N-terminal region couple to a mobile intersubunit interface. *Nature Communications.* **4** 1506 (2013).
13. Lau, K., & Van Petegem, F. Crystal structures of wild type and disease mutant forms of the ryanodine receptor SPRY2 domain. *Nature Communications.* **5** 5397 (2014).
14. Amador, F. J. *et al.* Crystal structure of type I ryanodine receptor amino-terminal beta-trefoil domain reveals a disease-associated mutation "hot spot" loop. *Proceedings of the National Academy of Sciences of the United States of America.* **106** (27), 11040-11044 (2009).
15. Lobo, P. A., & Van Petegem, F. Crystal structures of the N-terminal domains of cardiac and skeletal muscle ryanodine receptors: insights into disease mutations. *Structure.* **17** (11), 1505-1514 (2009).
16. des Georges, A. *et al.* Structural Basis for Gating and Activation of RyR1. *Cell.* **167** (1), 145-157 e117 (2016).
17. Efremov, R. G., Leitner, A., Aebersold, R., & Raunser, S. Architecture and conformational switch mechanism of the ryanodine receptor. *Nature.* **517** (7532), 39-43 (2015).
18. Peng, W. *et al.* Structural basis for the gating mechanism of the type 2 ryanodine receptor RyR2. *Science.* **354** (6310) (2016).
19. Wei, R. S. *et al.* Structural insights into Ca2+-activated long-range allosteric channel gating of RyR1. *Cell Research.* **26** (9), 977-994 (2016).
20. Yan, Z. *et al.* Structure of the rabbit ryanodine receptor RyR1 at near-atomic resolution. *Nature.* **517** (7532), 50-55 (2015).
21. Zalk, R. *et al.* Structure of a mammalian ryanodine receptor. *Nature.* **517** (7532), 44-49 (2015).
22. Furlong, M. J., Wright, D. J., & Dosdall, L. M. Diamondback moth ecology and management: problems, progress, and prospects. *Annual Review of Entomology.* **58** 517-541 (2013).
23. Amador, F. J. *et al.* Crystal structure of type I ryanodine receptor amino-terminal beta-trefoil domain reveals a disease-associated mutation "hot spot" loop. *Proceedings of the National Academy of Sciences of the United States of America.* **106** (27), 11040-11044 (2009).
24. Lobo, P. A., & Van Petegem, F. Crystal Structures of the N-Terminal Domains of Cardiac and Skeletal Muscle Ryanodine Receptors: Insights into Disease Mutations. *Structure.* **17** (11), 1505-1514 (2009).
25. Aslanidis, C., & de Jong, P. J. Ligation-independent cloning of PCR products (LIC-PCR). *Nucleic Acids Research.* **18** (20), 6069-6074 (1990).
26. Stepanov, S. *et al.* JBluIce-EPICS control system for macromolecular crystallography. *Acta Crystallographica Section D.* **67** (3), 176-188 (2011).
27. Minor, W., Cymborowski, M., Otwinowski, Z., & Chruszcz, M. HKL-3000: the integration of data reduction and structure solution--from diffraction images to an initial model in minutes. *Acta Crystallographica Section D.* **62** (Pt 8), 859-866 (2006).
28. McCoy, A. J. *et al.* Phaser crystallographic software. *Journal of Applied Crystallography.* **40** (Pt 4), 658-674 (2007).
29. Adams, P. D. *et al.* PHENIX: a comprehensive Python-based system for macromolecular structure solution. *Acta Crystallographica Section D.* **66** (Pt 2), 213-221 (2010).
30. Zwart, P. H., G.-K., R.W., Adams, P.D. Xtriage and Fest: Automatic assessment of X-ray data and substructure structure factor estimation. *CCP4 Newsletter.* (43), 27-35 (2005).
31. Kelley, L. A., Mezulis, S., Yates, C. M., Wass, M. N., & Sternberg, M. J. The Phyre2 web portal for protein modeling, prediction and analysis. *Nature Protocols.* **10** (6), 845-858 (2015).
32. Terwilliger, T. C. *et al.* Iterative model building, structure refinement and density modification with the PHENIX AutoBuild wizard. *Acta Crystallographica Section D.* **64** (Pt 1), 61-69 (2008).
33. Emsley, P., & Cowtan, K. Coot: model-building tools for molecular graphics. *Acta Crystallographica Section D.* **60** (Pt 12 Pt 1), 2126-2132 (2004).
34. Afonine, P. V. *et al.* Towards automated crystallographic structure refinement with phenix.refine. *Acta Crystallographica Section D.* **68** (Pt 4), 352-367 (2012).
35. Lin, L. *et al.* Crystal structure of ryanodine receptor N-terminal domain from Plutella xylostella reveals two potential species-specific insecticide-targeting sites. *Insect Biochemistry and Molecular Biology.* **92** 73-83 (2018).
36. Qi, S., & Casida, J. E. Species differences in chlorantraniliprole and flubendiamide insecticide binding sites in the ryanodine receptor. *Pesticide Biochemistry and Physiology.* **107** (3), 321-326 (2013).

